Repository Istituzionale dei Prodotti della Ricerca del Politecnico di Bari

Validation of FEM models based on Carrera Unified Formulation for the parametric characterization of composite metamaterials

(Article begins on next page)

09 March 2025

Validation of FEM models based on Carrera Unified Formulation for the parametric characterization of composite metamaterials

A.G. De Miguel[1], M. Cinefra[*2], M. Filippi[1], A. Pagani[1], E. Carrera[1]

(1) Department of Mechanical and Aerospace Engineering, Politecnico di Torino, Torino, Italy
(2) Department of Mechanics, Mathematics and Management, Politecnico di Bari, Bari, Italy

(*) Author and address for Correspondence
Prof. Maria Cinefra
Associate Professor,
Department of Mechanics, Mathematics and Management
Politecnico di Bari,
via Edoardo Orabona, 4,
70126 Bari, ITALY,
e.mail: maria.cinefra@poliba.it

Abstract

This work focuses on the study of composite metamaterials to be employed as possible lightweight insulation systems for noise and vibrations. In particular, the dispersion relations are derived by applying the Bloch-Floquet theory to the unit cell of the periodic microstructure. Advanced beam finite elements based on Carrera Unified Formulation are here extended, for the first time, to the dynamic characterization of these materials. Moreover, transmission curves are computed to validate the band gaps encountered in the analysis of dispersion behavior. The finite element model is first assessed by evaluating the dispersion behavior of some metamaterial configurations proposed in the literature. Finally, the model is applied to the parametric characterization of a composite metamaterial made of a melamine foam matrix and periodic distribution of cylindrical aluminium inclusions. The results show that it is possible to tune the band gaps of the metamaterial to lower frequencies by simply varying the dimensions of the unit cell and keeping constant its equivalent density.

1   Introduction

Since low-frequency mechanical and acoustic waves are especially difficult to absorb with conventional materials, due the order of magnitude of the wavelength, metamaterials have been recently proposed as broadband solution to the problem of noise and vibrations. This term refers to materials whose properties are "beyond" those of conventional materials. They are made from assemblies of multiple elements fashioned from composite materials such as metals, foams or plastics. The core concept of metamaterial is to replace the molecules with man-made structures called unit cell. They can be viewed as "artificial atoms", usually arranged in repeating patterns on a scale much less than the relevant wavelength of the phenomena they influence. Mechanical and acoustic metamaterials [1–5] are a category of metamaterials whose effective properties, like compressibility or density, can be negative. Negative density or compressibility can only be achieved dynamically. For instance, Helmholz Resonators driven just above their frequency of resonance lead to negative dynamic compressibility [6]. According to the same principles of wave propagation in periodic structures [7–9], metamaterials are tuned to the mechanical wavelength and can be categorized into non-resonant and resonant materials. In this field, an interesting research studying the properties of a composite material has been carried out at Virginia Tech in the past two decades [10, 11]. A similar configuration of metamaterial will be studied in this work.

One of the biggest challenges for the field of mechanical and acoustic metamaterials is the ability to identify, in a systematic and efficient way, structural geometries that endow metamaterials with desired functionalities. Many experimental studies have demonstrated unconventional properties through fabrication and testing of metamaterials designed ad-hoc. However, to design and predict the response of metamaterials, computational methods play a key role. The use of numerical models can provide a concise description of complex phenomena, such as dynamical behavior and/or large, quasi-static deformations. In particular, the finite element method (FEM) is a well-established approach in mechanics and yields accurate results for structural analysis of arbitrary geometrical shapes. The theoretical characterization of any periodic medium from a wave propagation standpoint, independently from the type of waves being studied, boils down to the computation of a 'dispersion relation', i.e. a relationship between wave properties, e.g. frequency and wavenumber. Its importance comes from the fact that one can capture the dispersion behavior of a periodic structure by simply analyzing the wave propagation behavior of its single repetitive volume element (RVE) under proper periodic boundary conditions [12–15]. This is fundamental, for example, if one wants to understand which frequencies are allowed to propagate and which ones are forbidden. Various techniques to obtain a dispersion relation are available in the literature, their common denominator being that they all leverage the Floquet-Bloch's principle. In simple terms, enforcing Bloch's principle is equivalent to imposing pe-

riodic boundary conditions to the wave problem: the unknowns (displacement or in the context of elastic/acoustic waves, electric field for electromagnetic waves) at certain locations on the boundary of the RVE are related to the same unknowns at different locations of the boundary via a complex exponential function of the components of the wave vector. Due to these boundary conditions, the periodic medium being treated has infinite dimensions: as a consequence, only structures in which the RVE is repeated "enough times" are accurately represented by these theoretical dispersion relations. Most of the methods provide the solution of an eigenvalue problem for the frequency as a function of the wavenumber. The FEM, in conjunction with Bloch's periodic boundary conditions, leads to approximate results, but its main advantage with respect to analytical methods is that it automatically enforces continuity of the degrees of freedom at material interfaces, if these coincide with elements' boundaries, allowing for the treatment of complicated one-, two- and three-dimensional geometries [16].

A novel approach based on FEM is here proposed for the dynamic characterization of periodic and composite metamaterials. It is based on the use of refined beam theories for the modeling of the microstructure and the derivation of the governing equations of the RVE. The Carrera Unified Formulation (CUF) is employed to generate higher-order beam models that show the same accuracy as conventional solid elements with reduced computational efforts. Accordingly, the main direction of the constituents (e.g. cylindrical inclusions in the composite metamaterial) is discretized by means of one-dimensional finite elements whereas the cross-section is hierarchically enriched with a set of interpolation polynomials with non-local capabilities. The validity of the proposed model is assessed through comparison with some benchmark solutions in terms of dispersion relations found in the literature and it is demonstrated its reduced computational cost with respect to classical 3D models in commercial codes. Finally, the model is applied to the parametric characterization of a composite metamaterial, made of melamine foam and periodic distribution of cylindrical aluminium inclusions, to be employed as possible lightweight insulation system for the reduction of noise and vibrations [17].

2   CUF modelling

The modelling approach here adopted is based on novel higher-order beam theories in the framework of the Carrera Unified Formulation and yields very accurate results with lower computational expenses, as demonstrated in the works [18,19]. The main advantage of CUF is that it allows to write the governing equations and the related finite element arrays in a compact and unified manner, which is formally an invariant with respect to the choice of the kinematic model. In this section, the mathematical derivation of the fundamental nuclei (the invariant) of the stiffness matrix and mass matrix in the case of CUF beam models is provided.

2.1   CUF beam models

To overcome the limitations of classical models and to deal with complex phenomena, such as wave propagation, the displacement field of a beam theory can be enriched with an arbitrary number of higher-order terms. The Carrera Unified Formulation (see [20,21]) exploits this possibility by describing the kinematic field in a unified manner that allows us to derive the governing equations in a very compact way. The displacement field of one-dimensional models in CUF framework is, in fact, described as a generic expansion of the generalized displacements (in the case of displacement-based theories) by arbitrary functions of the cross-section coordinates:

$$\mathbf{u}(x, y, z) = F_\tau(x, z)\mathbf{u}_\tau(y) \quad \tau = 1, 2, ..., M \tag{1}$$

where $\mathbf{u}_\tau$ is the vector of general displacements, M is the number of terms in the expansion, τ denotes summation and $F_\tau(x, z)$ defines the 1D model to be used. In fact, depending on the choice of $F_\tau(x, z)$

3

functions, different classes of beam theories can be implemented. Among these, Lagrange Expansions (LE) beam theories are employed in this work.

(a) Approximation over the cross-section (CUF)

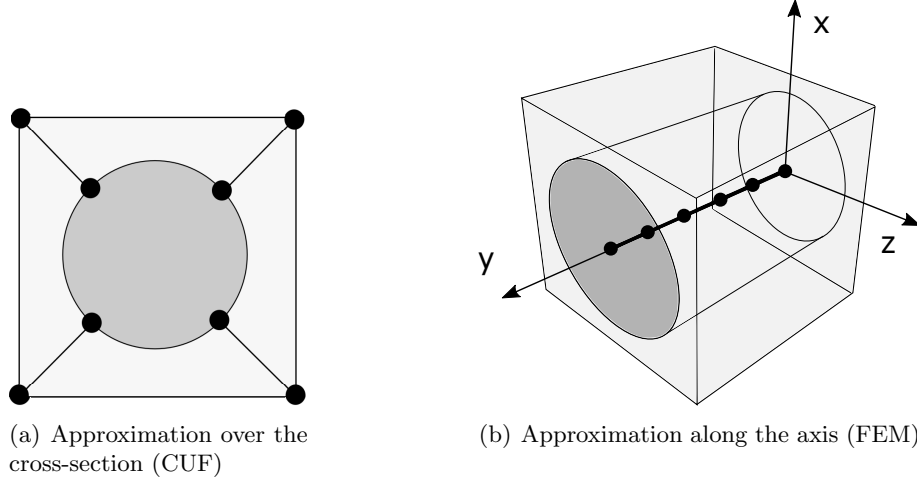(b) Approximation along the axis (FEM)

Figure 1: An example of discretization of the unit cell using CUF beam finite elements: the nodes along the axis illustrated in (b) represent the positions at which the nodes over the cross-section shown in (a) are repeated, for a total of 8×6 physical nodes.

LE theories use Lagrange-type polynomials as generic functions over the cross-section. The cross-section is therefore divided into a number of local expansion sub-domains, whose polynomial degree depends on the type of Lagrange expansion employed: three-node linear L3, four-node bilinear L4, nine-node cubic L9, and sixteen-node quartic L16 polynomials can be used to formulate refined beam theories (see Carrera and Petrolo [22]). In Figure 1(a) the cross-section is divided in four sub-domains, in which four-node bilinear L4 polynomials are used.

For example, the interpolation functions of a L9 expansion are defined as:

$$
\begin{aligned}
F_\tau &= \tfrac{1}{4}(r^2 + r\,r_\tau)(s^2 + s\,s_\tau) \qquad \tau = 1,3,5,7 \\
F_\tau &= \tfrac{1}{2}s_\tau^2(s^2 + s\,s_\tau)(1 - r^2) + \tfrac{1}{2}r_\tau^2(r^2 + r\,r_\tau)(1 - s^2) \qquad \tau = 2,4,6,8 \\
F_\tau &= (1 - r^2)(1 - s^2) \qquad \tau = 9
\end{aligned}
\tag{2}
$$

where r and s are natural coordinates that vary over each sub-domain of the cross-section between -1 and $+1$, and r_τ and s_τ represent the locations of the roots in the natural plane. The kinematic field of the single-L9 beam theory is therefore

$$
\begin{aligned}
u_x &= F_1\,u_{x_1} + F_2\,u_{x_2} + F_3\,u_{x_3} + ... + F_9\,u_{x_9} \\
u_y &= F_1\,u_{y_1} + F_2\,u_{y_2} + F_3\,u_{y_3} + ... + F_9\,u_{y_9} \\
u_z &= F_1\,u_{z_1} + F_2\,u_{z_2} + F_3\,u_{z_3} + ... + F_9\,u_{z_9}
\end{aligned}
\tag{3}
$$

Refined beam models can be obtained by adopting higher order Lagrange polynomials or by using a combination of Lagrange polynomials on multi-domain cross-sections. More details about Lagrange-class beam models can be found in [22–25].

2.2 Finite element formulation

Let the 3D displacement vector be defined as:

$$
\mathbf{u}(x, y, z) = \left\{ \begin{array}{c} u_x(x, y, z) \\ u_y(x, y, z) \\ u_z(x, y, z) \end{array} \right\}
\tag{4}
$$

4

According to classical elasticity, stress and strain tensors can be organized in six-term vectors with no lack of generality. They read, respectively:

$$\boldsymbol{\sigma}^T = \{\ \sigma_{yy} \quad \sigma_{xx} \quad \sigma_{zz} \quad \sigma_{xz} \quad \sigma_{yz} \quad \sigma_{xy}\ \}$$
$$\boldsymbol{\varepsilon}^T = \{\ \varepsilon_{yy} \quad \varepsilon_{xx} \quad \varepsilon_{zz} \quad \varepsilon_{xz} \quad \varepsilon_{yz} \quad \varepsilon_{xy}\ \} \tag{5}$$

Regarding to this expression, the geometrical relations between strains and displacements with the compact vectorial notation can be defined as:

$$\boldsymbol{\varepsilon} = \mathbf{D}\,\mathbf{u} \tag{6}$$

where, in the case of small deformations and angles of rotations, $\mathbf{D}$ is the following linear differential operator:

$$\mathbf{D} = \begin{bmatrix} 0 & \frac{\partial}{\partial y} & 0 \\ \frac{\partial}{\partial x} & 0 & 0 \\ 0 & 0 & \frac{\partial}{\partial z} \\ \frac{\partial}{\partial z} & 0 & \frac{\partial}{\partial x} \\ 0 & \frac{\partial}{\partial z} & \frac{\partial}{\partial y} \\ \frac{\partial}{\partial y} & \frac{\partial}{\partial x} & 0 \end{bmatrix} \tag{7}$$

On the other hand, for orthotropic materials the relation between stresses and strains is obtained through the well-known Hooke's law:

$$\boldsymbol{\sigma} = \mathbf{C}\,\boldsymbol{\varepsilon} \tag{8}$$

where $\mathbf{C}$ is the matrix of elasticity coefficients:

$$\mathbf{C} = \begin{bmatrix} C_{33} & C_{23} & C_{13} & 0 & 0 & 0 \\ C_{23} & C_{22} & C_{12} & 0 & 0 & 0 \\ C_{13} & C_{12} & C_{11} & 0 & 0 & 0 \\ 0 & 0 & 0 & C_{44} & 0 & 0 \\ 0 & 0 & 0 & 0 & C_{55} & 0 \\ 0 & 0 & 0 & 0 & 0 & C_{66} \end{bmatrix} \tag{9}$$

and these depend on the Young's moduli, the shear moduli and the Poisson ratios of the orthotropic material.

The discretization along the longitudinal axis of the beam is made by means of the finite element method (see Figure 1(b)). The generalized displacements are in this way described as functions of the unknown nodal vector, $\mathbf{q}_{\tau i}$, and the 1D shape functions, N_i.

$$\mathbf{u}_\tau(y) = N_i(y)\mathbf{q}_{\tau i}, \qquad i = 1, 2, ..., n_{elem} \tag{10}$$

where n_{elem} is the number of nodes per element and the unknown nodal vector is defined as

$$\mathbf{q}_{\tau i} = \{\ q_{u_{x\tau i}} \quad q_{u_{y\tau i}} \quad q_{u_{z\tau i}}\ \}^T \tag{11}$$

Different sets of polynomials can be used to define FEM elements. Lagrange interpolating polynomials have been chosen in this work to generate cubic one-dimensional elements. For the sake of brevity, their expression is not provided, but it can be found in the book by Carrera et. al [21], in which two-node (B2), three-node (B3) and four-node (B4) elements are described.

The governing equations for free vibration analysis are obtained via the Principle of Virtual Displacements (PVD). This variational statement sets as a necessary condition for the equilibrium of a

structure that the virtual variation of the internal work (left hand side) has to be the same as the virtual variation of the inertial work (right hand side), or:

$$\int_l \int_\Omega \delta\boldsymbol{\varepsilon}^T \boldsymbol{\sigma} \, d\Omega \, dy = \int_l \int_\Omega \delta\mathbf{u}^T \rho \, \ddot{\mathbf{u}} \, d\Omega \, dy \tag{12}$$

where l stands for the length of the beam and Ω is the cross-section domain; ρ stands for the density of the material, and $\ddot{\mathbf{u}}$ is the accelerations vector. By adopting the geometrical relation (Eq. (6)), the constitutive law (Eq. (8)), the CUF kinematic field (Eq. (1)) and the FEM discretization (Eq. (10)), the equilibrium equations can be rewritten as:

$$\delta\mathbf{q}_{\tau_i}^k : \quad \mathbf{K}^{k\tau sij}\mathbf{q}_{s_j}^k = \mathbf{M}^{k\tau sij}\ddot{\mathbf{q}}_{s_j}^k \tag{13}$$

$\mathbf{K}^{k\tau sij}$ and $\mathbf{M}^{k\tau sij}$ are 3×3 matrices, called fundamental nuclei of stiffness and mass matrix, respectively, and their explicit expression is given in previous authors works [26]. These are the basic elements from which the stiffness matrix and mass matrix of the whole structure is computed. The fundamental nuclei are expanded on the indexes τ and s in order to obtain the matrices of each element. Then, the matrices of the elements are assembled according to the classical finite element procedure. For more details about the derivation of governing equations, the reader can refer to the article [27]. The final form of the free-vibration problem can be written as it follows:

$$-\mathbf{M}\ddot{\mathbf{q}} + \mathbf{K}\mathbf{q} = 0 \tag{14}$$

where $\mathbf{q}$ is the vector of the nodal displacements. Introducing harmonic solutions, it is possible to compute the natural frequencies ω_l, by solving an eigenvalues problem:

$$-(\omega_l^2 \mathbf{M} - \mathbf{K})\mathbf{q}_l = 0 \tag{15}$$

where $\mathbf{q}_l$ is the l-th eigenvector.

3 Dispersion relations

The FEM, in conjunction with Bloch's periodic boundary conditions, leads to a formulation that allows us to calculate the dispersion relations of the discretized RVE. The main advantage of the FE-based method is that it automatically enforces continuity of the degrees of freedom at material interfaces, if these coincide with elements' boundaries, allowing for the treatment of complicated one-, two- and three-dimensional geometries.

Let us consider the 1D case to start the derivation of dispersion relations by grouping the degrees of freedom of the discretized RVE in the following vector:

$$\mathbf{q} = \{\mathbf{q}_0, \mathbf{q}_i, \mathbf{q}_L\}^T \tag{16}$$

where $\mathbf{q}_0$ are the nodal displacements at left-side of the RVE and $\mathbf{q}_L$ are the nodal displacements at right-side. $[\mathbf{q}_i]$ contains all the degrees of freedom of the internal nodes (all the nodes apart from the boundary ones). The displacements $\mathbf{q}_0$ and $\mathbf{q}_L$ are related through the Bloch condition $\mathbf{q}_L = e^{-i\mathbf{k}} \mathbf{q}_0$, where $\mathbf{k}$ is the wave vector with components (k_x, k_y, k_z). This allows to formulate the reduced vector of degrees of freedom:

$$\mathbf{q}_r = \{\mathbf{q}_0, \mathbf{q}_i\}^T \tag{17}$$

$\mathbf{q}$ and $\mathbf{q}_r$ are then related through $\mathbf{q} = \mathbf{W}\mathbf{q}_r$, where $\mathbf{W}$ is defined as:

$$\mathbf{W} = \begin{bmatrix} \mathbf{I}_{1\times 1} & \mathbf{0}_{1\times in} \\ \mathbf{0}_{in\times 1} & \mathbf{I}_{in\times in} \\ e^{-i\mathbf{k}}\mathbf{I}_{1\times 1} & \mathbf{0}_{1\times in} \end{bmatrix} \tag{18}$$

where $\mathbf{I}$ and $\mathbf{0}$ are identity and null matrices, respectively. The dimensions of the sub-matrices are reported as pedices and in is the number of internal degrees of freedom. A reduced eigenproblem is now formulated as:

$$\left(\mathbf{W}^H \mathbf{K} \mathbf{W} - \omega^2 \mathbf{W}^H \mathbf{M} \mathbf{W}\right) \mathbf{q}_r = 0 \tag{19}$$

where the H apex stands for Hermitian transpose. Eq. (19) represents the eigenvalue problem to be solved to determine the dispersion relation. In particular, values of ω will be obtained by specifying values for the wavenumbers k_x, k_y, k_z. Due to periodicity, it is enough to specify values of wavenumbers that belong to the First Brillouin zone of the RVE [28].

The straight-forward applicability of this method to higher-dimensional problems is what makes it very powerful. If a 2D or 3D periodic medium is considered, one has to choose the RVE properly and has to identify the lattice vectors, i.e. the vectors that are used to connect any point in the RVE to the same point in a neighboring cell. Moreover, when applying Bloch's conditions, the components of the wave vector along these lattice vectors have to be considered. Taking into account the FEM approximation, the lowest-frequency branches of dispersion relations are well-characterized by a relatively coarse model; refining the mesh leads to a dispersion relation that, also at high frequencies, converges to the exact one.

4   Assessment of the model

The aim of this study case is to assess the proposed modeling technique for the detection of band gaps in locally resonant metastructures. For this purpose, the well-known example of Wang et al. [29] is studied first. The metamaterial consists of a 2D array of ternary locally resonant phononic crystals. This class of periodic structure was introduced for vibration control and noise insulation, and it is composed by cylindrical scatterers with uniform coatings in their exterior. It is found that a complete band gap is generated at low frequencies where the elastic wave propagation is prohibited. Contrarily to the band gaps that appear due to Bragg scattering effects, local resonances induce this effect at the low frequency spectrum, which can be interesting for certain structural and acoustic applications. Indeed, the authors in [29] show that the frequency ranges of the band gap can be tuned by varying the elastic modulus of the coating.

4.1   Dispersion curves of the infinite metamaterial

The ternary phononic crystal studied here consists of a 2D periodic array of cells made of a cylindrical metal core coated by rubber and embedded in the polymer matrix. The material properties used for the analysis are enlisted Table 1. The geometry of the cell is shown in Fig. 2 (a), where: r_1 is the core radius and r_2 is the outer diameter of the coating. The dimension of the cell respect the following relations:

$$\frac{r_1}{a} = 0.27 \qquad \frac{r_2}{a} = 0.4. \tag{20}$$

The effective geometrical dimensions used in this example are provided $a = 20.1 \, mm$, $r_1 = 5.427 \, mm$ and $r_2 = 8.04 \, mm$.

Table 1: Unit cell materials properties [29].

	Core	*Coating*	*Matrix*
$E[\text{Pa}]$	$2.1 \cdot 10^{11}$	$1 \cdot 10^5$	$3.5 \cdot 10^7$
ν	0.29	0.47	0.49
$\rho[\text{kg m}^{-3}]$	8950	1020	1200

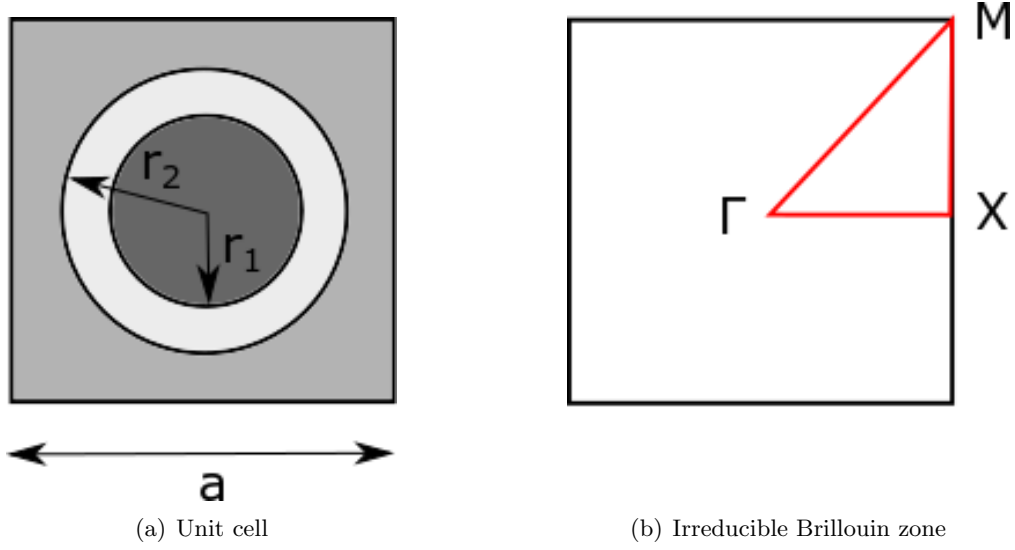(a) Unit cell   (b) Irreducible Brillouin zone

Figure 2: Geometry of the unit cell and representation of the irriducible Brillouin zone [30].

The dispersion properties of the metamaterial are computed using the Bloch boundary conditions and varying the wave vector over the irreducible Brillouin zone, which is marked by the red path $(\Gamma - X - M)$ in Fig. 2 (b). Due to the double symmetry of the lattice, this triangular area is sufficient to describe the wave propagation behavior of the metamaterial.

According to [29], the band structure is characterised by a particular expression for the reduced frequency:

$$\Omega = \frac{\omega a}{2\pi c_t} \tag{21}$$

where c_t is the transverse wave velocity of the matrix material and it is:

$$c_t = \sqrt{\frac{E}{\rho}} = 170.7825128 \frac{m}{s} \tag{22}$$

Figure 3 shows a detail of the dispersion curves accounting for the first modes only, showing the existence of a broad band gap. The results are in very good agreement with those of the reference paper [29]. The locally resonant nature of this band gap is demonstrated by the fact that the lower and upper edge frequencies are shifted. The correspondent modes of the extreme frequencies are also shown in Fig. 3. As described in the reference paper, at the lower edge of the band gap the core oscillates as a rigid sphere and the coating acts as a spring. On the other hand, at the upper edge of the band gap the core and the matrix oscillate in a reverse phase. For the sake of completeness, Fig. 4 reports the complete dispersion curve including also higher-order modes.

4.2   Elastic wave transmission

In order to complement the dynamic analysis of the infinite metamaterial performed in the previous step, a frequency response analysis is now carried out over a finite strip of eight cells placed over the x-direction. This exercise serves also as a further verification of the existence of the lower band gap for the locally resonant structure under study. Figure 5 shows the section mesh of the model and the boundary conditions. A unitary displacement is imposed over the nodes of the left-end edge, denoted as edge 1, and the displacement transmitted is evaluated at the opposite end, denoted as edge 2. Periodic conditions are imposed over the top and bottom edges. The transmission coefficient (TC) is calculated
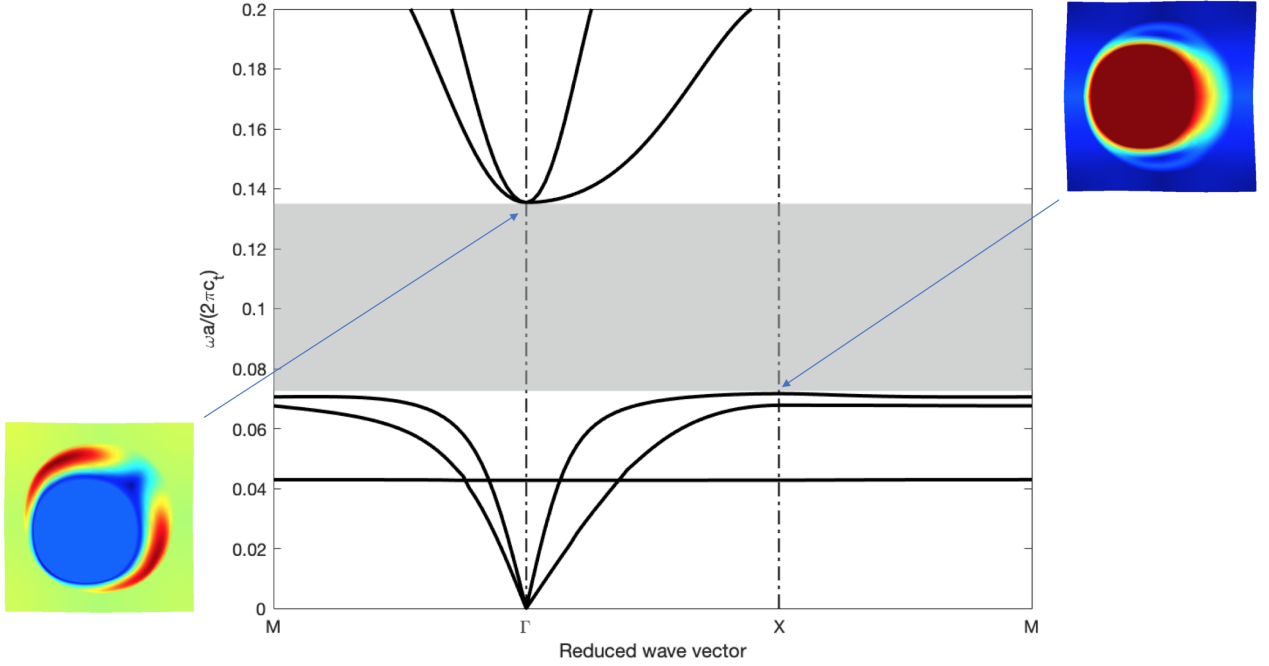
Figure 3: Detail of the dispersion curves showing band gap edge modes.

as

$$\text{TC} = \log_{10}\left(\frac{\int_0^a |u_2| dz}{\int_0^a |u_1| dz}\right) \tag{23}$$

where:

- $|u_2|$ is the amplitude of the transmitted wave;

- $|u_1|$ is the amplitude of the incident wave.

Two excitations are accounted for: an x-polarized wave, i.e. pressure wave; and a z-polarize wave, i.e. shear wave. These two excitations are modeled numerically by imposing horizontal and vertical unitary displacements, respectively. Figure 6 shows the transmission curves for both pressure and shear waves for a range of frequencies between 0 and 5000 Hz. It is possible to observe that for the section between 500 to 820 Hz there is a clear decay of the transmission for both wave types. The agreement of these results with the band gap shown by the dispersion curves in the infinite metamaterial is demonstrated. In addition, the transmission curves provide information about the effectiveness of the structure to mitigate the propagation of elastic waves.

A detail of the transmission curves with some relevant modes for the pressure and shear excitations is shown in Figs. 7 and 8, respectively. The contour of the right-hand side plots represents the displacement amplitude over the finite strip of metamaterial. For the pressure wave, the transmission coefficient shows a sharp peak at 537.5 Hz. At that frequency, it can be seen that most of the energy is contained at the first cell through the local resonance of the core. After the peak, the propagation of the excitation is steadily recovered. A similar behavior is observed for the shear wave, although in this case the decay of the transmission coefficient begins at slightly lower frequencies and the propagation is recovered abruptly after a wider zone of decay peaks.
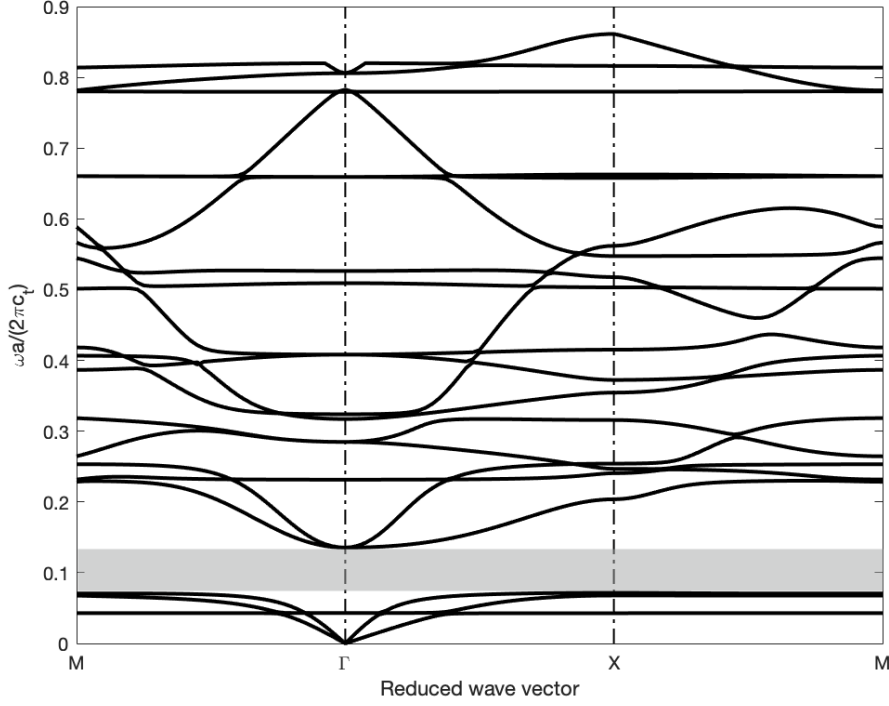
9

Figure 4: Fully reduced dispersion curves obtained by the present CUF model.

5   Melamine-Aluminum metamaterial

The metamaterial here considered for the parametric study is defined as a composite system consisting of multiple small masses embedded within a passive poro-elastic matrix material. The embedded masses create an array of resonant mass-spring-damper systems within the material that operate at low frequencies where the passive poro-elastic material is no longer effective. By employing the poro-elastic material to provide the stiffness for the embedded masses, the metamaterial utilizes two passive control schemes: damping at high frequencies, and dynamic absorption at low frequencies, into a single device for broadband insulation.

Many works are devoted to the study of internal treatments for the attenuation of low-frequency noise and vibrations, especially in the aeronautical field [31–34]. In this context, the metamaterials can be used for controlling low frequency sound radiation, improving low frequency transmission loss when attached to vibrating structures, and they are a lighter replacement to conventional materials as demonstrated by the authors in [17]. In [35], the authors also show that composite metamaterials can be used as lightweight blanket treatments for effectively controlling low frequency sound radiating from structure in the cabin of aircraft, according to the concept anticipated in the works [36,37]. This application is largely dictated by the choice of the poro-elastic and the inclusion materials on the basis of the aeronautical standards (all the details about the identification of constituent materials are provided in [17]). Therefore, the periodic unit-cell of the metamaterial here considered is represented in Figure 9 and it is made of melamine matrix and aluminium cylindrical inclusions. The metamaterial plate is constructed over the (2,3)-plane, and the axis 1 corresponds to the thickness direction.

Let us define the volume fraction V_f as the ratio between the volume of the inclusion and the entire volume of the unit cell, so it is depending only on the diameter of the inclusion and the side length of the cell and is independent from the thickness. According to that, for a unit cell with side a, the diameter
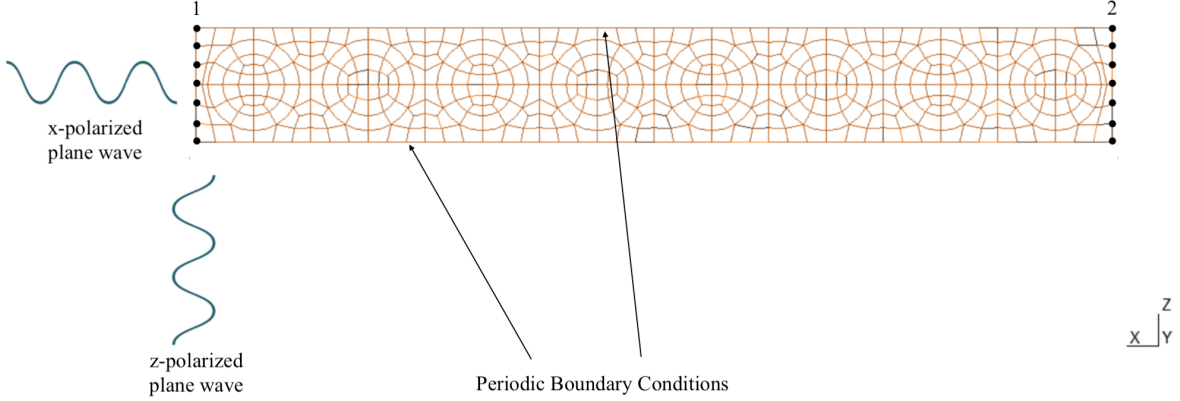
Figure 5: Transmission curves analysis set up.

of the cylindrical inclusion is calculated as: $d = \sqrt{\frac{V_f}{\pi}} \times 2a$. The melamine density is approximated to be $\rho_M = 8\,\text{kg/m}^3$ which appears to be the low average for this material; the aluminium density is $\rho_{\text{Al}} = 2700\,\text{kg/m}^3$. The equivalent density ρ_{eff} of the metamaterial can be computed by the formula $\rho_{\text{eff}} = \rho_M(1 - V_f) + \rho_{\text{Al}}V_f$.

After the assessment in the previous section, the following analyses will be focused on the dynamic characterization of the composite metamaterial. Due to the high differences in elastic moduli and density between the melamine foam and the aluminum inclusions, an elastic band gap due to local resonances is expected at low frequencies (0-1000 Hz).

This material system presents some complexities that must be carefully addressed prior running the analyses. The melamine foam is usually modeled as a viscoelastic orthotropic material, which is characterized by frequency-dependent real and imaginary moduli [17]. However, for simplicity reasons, in this preliminary design the melamine is defined as an elastic orthotropic foam with zero viscosity. This choice is supported by the fact that, as it is observed in many works such as [30], the increase of the viscosity exhibits an almost negligible effect on the band gap frequencies, which is the main target of this research. As a consequence of this assumption, a direct solver can be used and only the real part of the system is studied. Therefore, the mechanical properties of the melamine foam, as used in the subsequent analyses, are included in Table 2, which are calculated as an average over a range of frequencies between 0 Hz and 4000 Hz (for the derivation of melamine mechanical properties, the readers can refer to the article [17]). Note that, according to several studies [38, 39], the variation of the real part of the melamine properties at low frequencies is fairly small. Finally, the Aluminium has isotropic properties $E = 6.75 \times 10^{10}$ Pa and $\nu = 0.34$.

Table 2: Properties of melamine.

$\rho[\text{Kg/m}]$	$E_1[\text{Pa}]$	$E_2[\text{Pa}]$	$E_3[\text{Pa}]$	$G_{12}[\text{Pa}]$	$G_{23}[\text{Pa}]$	$G_{13}[\text{Pa}]$	ν_{12}	ν_{23}	ν_{13}
8.0	$4.590 \cdot 10^5$	$2.161 \cdot 10^4$	$1.742 \cdot 10^5$	$1.037 \cdot 10^5$	$1.063 \cdot 10^5$	$1.270 \cdot 10^5$	0.445	0.433	-0.514

Since this material has been conceived to be used as core of the sandwich lining panels of aircrafts, and its lightness is a requirement [17], the equivalent density of the metamaterial is imposed to have a constant value near the density of the Nomex ($48\ kg/m^3$), being this a material commonly used in aeronautics. Consequently, the volume fraction between the inclusions and the foam is chosen in order
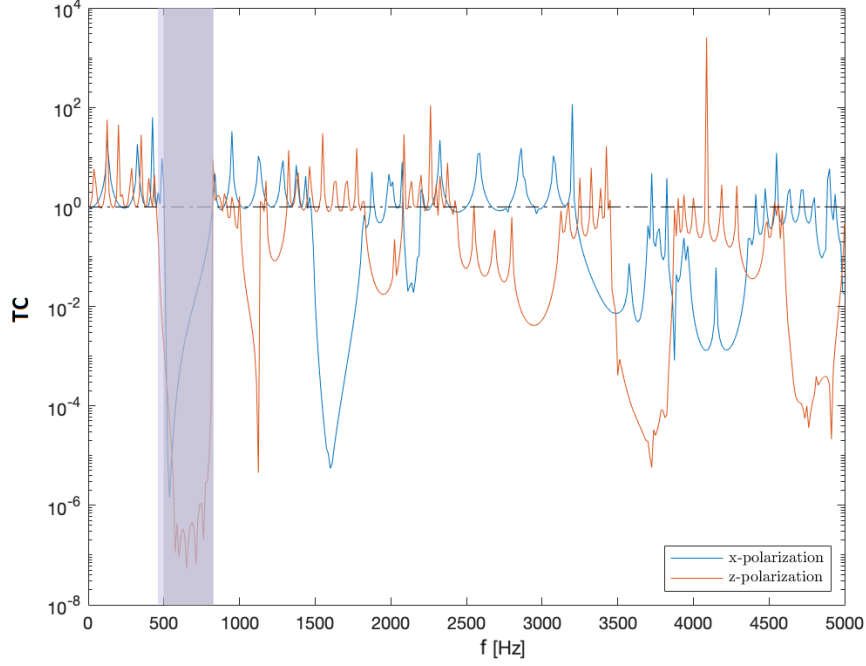
Figure 6: Transmission curves for both pressure and shear waves.

to comply this condition. An initial dimension of the cell is assigned: the corresponding geometrical characteristics of the unit cell are $a = 3\,cm$, $d = 4\,mm$ and the volume fraction is $V_f = 0.01396$. The equivalent density of the metamaterial is $37.8\,\mathrm{Kg/m^3}$. When increasing the in-plane dimensions of the unit cell (the thickness is kept constant), the number of the unit cells must be decreased in order to keep constant the mass of the panel. Since the dimensions of aeronautical panel are big enough to include hundreds of unit cells even in the case of large unit cells (12 cm), the effect of the periodicity can be still considered.

The beam model generated for the present simulation consists of a single element in the thickness direction and a mesh of 52 quadratic domains (L9 elements) over the section, as it is shown in Fig. 10. The same analyses described in the previous example are performed again. The aim is to first demonstrate the existence of local resonance behaviors in the material system and to characterize the resultant band gaps. Secondly, the cell dimension is modified to prove the design flexibility of such metamaterials for elastic wave absorption. The idea is that by varying a certain design parameter it is possible to shift the band gap to different frequency ranges while keeping the same equivalent density of the structural plate.

The authors have to underline that, for some reasons that will be provided in the next section, the analyses performed on this metamaterial . However, the authors are aware that the transmission of acoustic waves in the through-thickness direction of the aircraft sidewalls is very important for the evaluation of noise reduction inside the cabin and it will be studied

5.1   Comparison with 3D model

Although the beam elements based on CUF present 3D capabilities deriving from the use of Lagrangian interpolating functions over the cross-section, we have validated the CUF model by comparison with 2D solutions provided in literature mainly because 3D solutions were not available for unit cells sim-
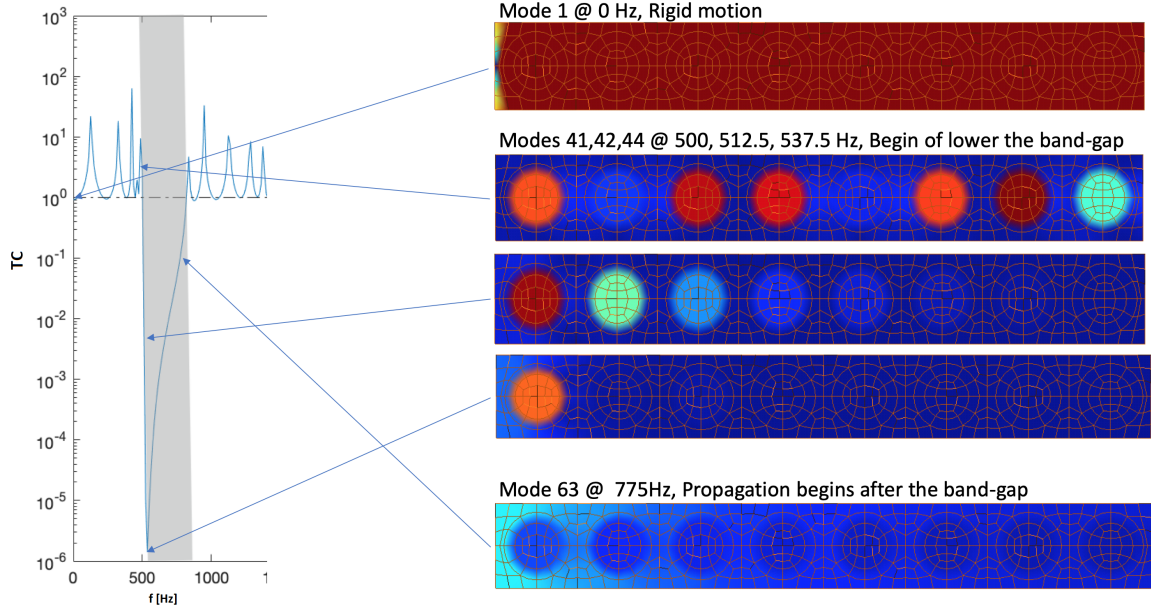
Figure 7: Detail of the transmission curve for a x-polarized plane wave, showing most important modes shapes.

ilar to that one of our interest. Moreover, we don't expect any band gap through the thickness of the metamaterial here proposed and, for these reasons, the results provided in the following sections consider only in-plane propagation of elastic waves. Taking into account the aeronautical application, the transmission of acoustic waves in the through-the-thickness direction of the aircraft sidewalls might be relevant for the evaluation of noise reduction inside the cabin. However, the 3D dispersion analysis deserves a separated work, because the CUF model needs to be validated by comparison with an ad-hoc 3D model created with commercial software, which remains out of the scope of the purposes of the present research.

The main objective of this work is the extension of the CUF to the characterization of generic meta-materials, not only 2D. In order to show the 3D capabilities of the proposed CUF beam elements, a comparison with a 3D model created with a commercial software (Ansys) is presented in this section. For further details on the computational advantages of similar approaches the reader is referred to [18, 40–44]. In this manner, the 3D-like model of the unit cell is also validated.

A free-vibration analysis of the unit cell is performed using both the present CUF model and the 3D model created in Ansys (Figure 11). No boundary conditions are applied to the unit cell. The first 30 natural frequencies are computed and compared in Table 3. After a convergence study, it has been established that 16821 eight-node 3D elements and 59160 degrees of freedom (dofs) are required in Ansys to get the exact solution, while only 2798 dofs are used in CUF beam model. The small differences between the two solutions (less than 1%) are attributable to numerical reasons that go beyond the CUF modelling. The perfect agreement between the solutions at higher frequencies, where 3D mode shapes can appear (see Figure 12), demonstrates the 3D capabilities of our model. Being the dispersion relations and transmission curves the reiterated computation of the same dynamic system of the free-vibration analysis, one can estimate the enormous computational advantage of using the present model in the parametric study of metamaterials.
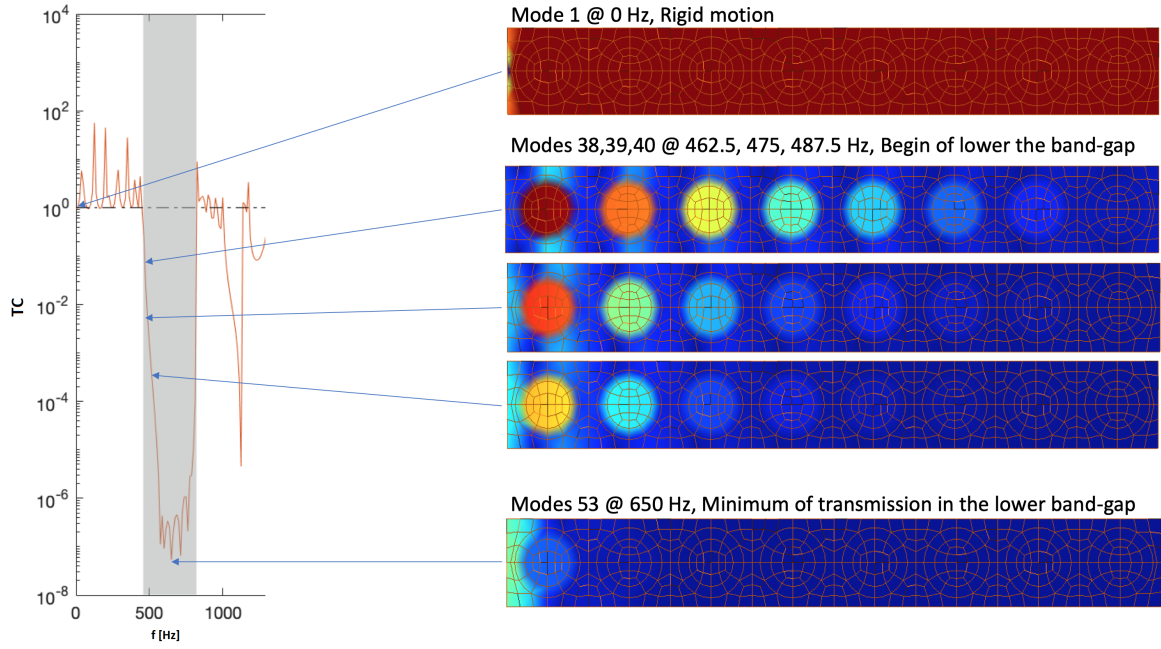
13

Figure 8: Detail of the transmission curve for a z-polarized plane wave, showing most important modes shapes.

5.2 Dispersion Curves

The dispersion curves obtained with the melamine-aluminum cell are plotted in Fig. 13 together with the images of the most relevant modes. Note that, due to the orthotropy of the melamine foam, the metamaterial behaves differently in the x and z directions. For this reason, the first Brillouin zone must be enlarged to account also for the variation of the wave vector over the z-axis. Thus the dispersion curves are computed over $\Gamma - X_1 - M - X_2$, as it is shown in the detail of Fig. 13.

From the graph it is possible to observe that the 3rd mode is almost constant across the entire Brillouin zone, meaning that it barely propagates. Indeed, the correspondent mode shape shows that it consists of an internal rotation of the aluminum inclusion with a local deformation of the melamine foam. Therefore the effective band gap is due to the local resonance of the inclusion and is located between modes 2 and 4, which are also shown in Fig. 13 (bottom and top, respectively). The range of frequencies in which the elastic wave propagation is mitigated goes from 1040 Hz up to 2830 Hz.

5.3 Transmission Curves

In order to confirm the existence of a band gap at low frequencies due to local resonances, the frequency response analysis of the finite metamaterial is also carried out. As it was done for the first assessment, a strip of eight cells is modeled to evaluate the propagation of pressure and shear wave excitations over the 2D pattern. The results are included in Fig. 14, which shows the transmission coefficient for a range of frequencies between 0 and 8000 Hz. One can see that the TC decays greatly for both excitations in correspondence to the band gap frequencies. For clarity reasons, the band gap computed from the dispersion curves is included in the plot as a shaded area.

Figure 15 includes some relevant modes which are obtained from the present analysis at two different frequencies: 792 Hz (below the band gap) and 1592 (inside the band gap). First, one can observe that all the propagation modes are dominated by the movement of the aluminum inclusion in the melamine matrix, as shown in Figs. 15 (a) and (c). Moreover, the existence of local resonances in the metamaterial
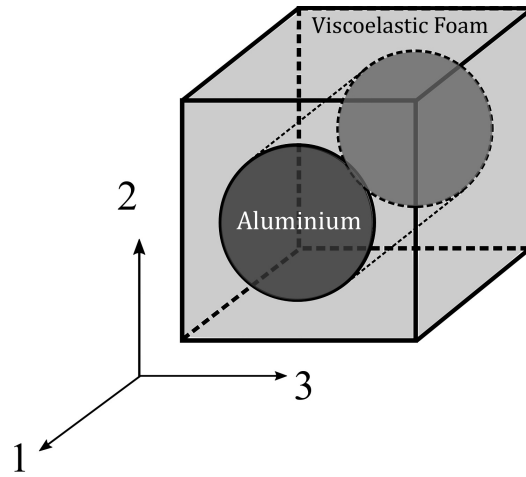
14

Figure 9: Periodic Unit Cell of the Metamaterial with matrix of melamine foam and cylindrical inclusions of Aluminium.
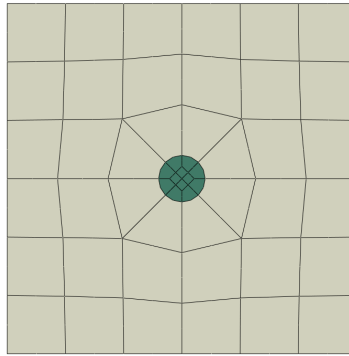

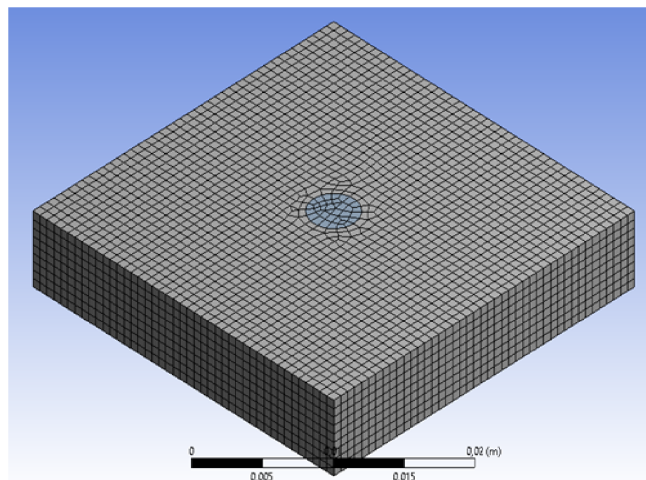Figure 10: FEM model of metamaterial cell using CUF beam models.
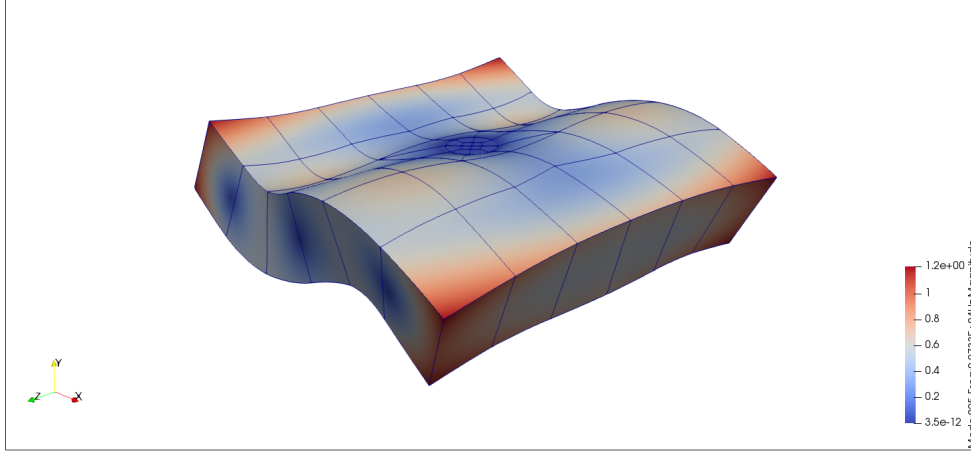

Figure 11: 3D model created in Ansys.

Figure 12: CUF model: 25th mode shape of the unit cell (Melamine+Aluminium).

cell is also proved by Figs. 15 (b) and (d). In fact, for both pressure and shear excitations, at 1592 Hz the elastic waves stop already at the first cell due to the out-of-phase movement of the inclusion.

5.4   Parametric study

Finally, a parametric study is performed to study the variation of the band gap size and range for different values of the cell dimension, *a*. Note that the volume fraction of the metamaterial system is maintained constant, thus the diameter of the particle is also increased proportionally. It is expected that the variation of the local masses of the aluminum will shift the band gap frequencies, while the overall weight of the plate remains unaltered.

The results of this study are shown in Fig. 16. It includes the lower and upper edges of the band gap for *a* values varying from 1 cm to 12 cm. The gap between these two curves is shown in grey for clarity. Also, the minimum and maximum band gap frequencies for each test case conducted are written between brackets. The results show that the total band gap size diminishes as the unit cell is enlarged. Moreover, it shows that the mitigated frequencies shift to lower values, demonstrating that it is possible to create band gaps which cover a wide range of frequencies below 1000 Hz.

It is worth noting that, when dealing with bigger unit cells or larger metamaterial structures, the viscoelastic characteristics may not be negligible. On this regard, the study of the frequency-dependent problem requires the implementation of shift cell techniques in the framework of CUF and will be addressed in future extensions of the model.

6   Conclusions

In this work, composite metamaterials have been dynamically characterized by the computation of dispersion relations. The finite element method has been employed and, in particular, the advanced beam finite elements based on CUF have been extended for the first time to the analysis of dispersion behavior in periodic materials according to the Bloch-Floquet theory. Also the transmission of waves through a chain of unit cells has been evaluated to validate the band gaps found. The model has been successfully assessed through the study of a locally resonant metamaterial from the literature. Then, the method has been applied to the analysis of the metamaterial of our interest. Finally, a parametric study has been carried out to show that the band gap of the metamaterial can be shifted to lower frequencies by increasing the dimensions of the unit cell and keeping constant both the volume fraction of the inclusions and the equivalent density of the material.
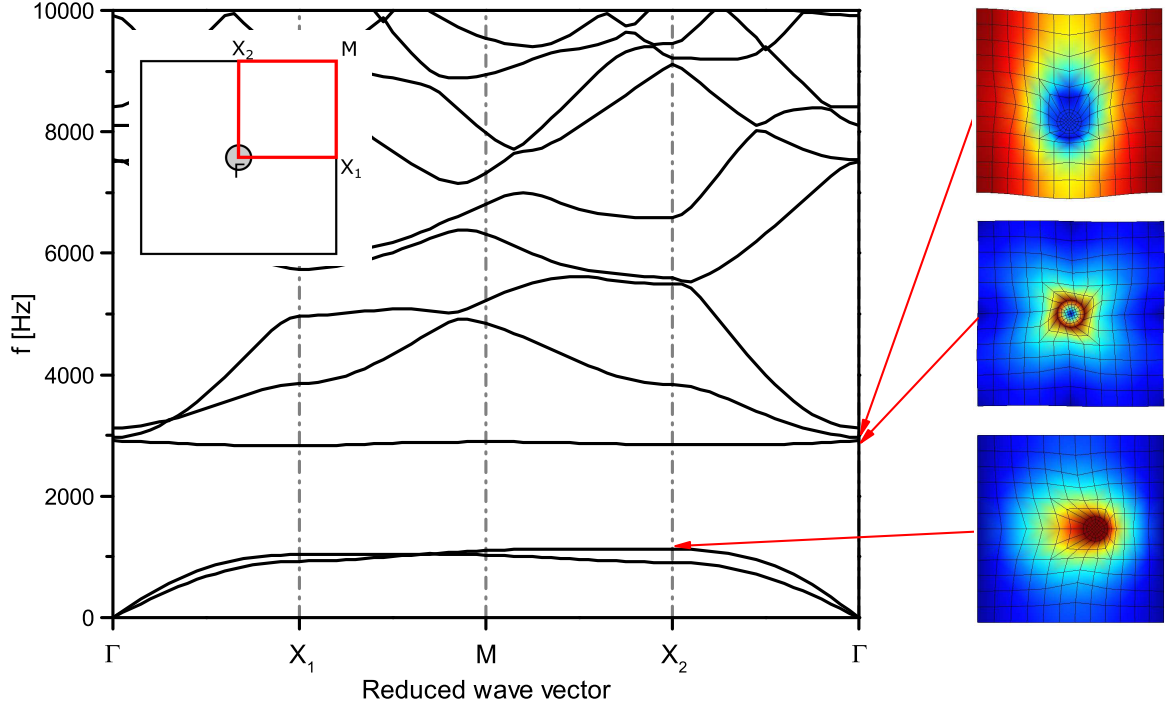
Figure 13: Dispersion curves of the melamine-aluminum metamaterial in the first Brillouin zone, which is illustrated in the upper left corner of the graph.

Therefore, this study shows that there is a real potential for the design of metamaterials for applications in which it is difficult to absorb low frequencies without increasing the weight of the structure. Such kind of materials can be used for instance to mitigate the structural vibrations that have a detrimental effect on the levels of comfort inside the cabin of aircraft. In fact, recent research studies prove that similar structures can be used to increase the sound transmission loss [45] in air-borne environments. Anyway, the introduction of new manufacturing techniques, such as 3D-printers, enables the study of more complex metamaterials, allowing the designers to explore more efficient solutions. To this aim, the advanced finite elements based on the CUF will allow us to perform the numerous analyses with high accuracy and lower computational time with respect to commercial softwares. The final objective is to develop an efficient modeling tool that will provide an high-fidelity simulation of integrated meta-material components for a design approach aimed to the practical implementation of this promising technology.
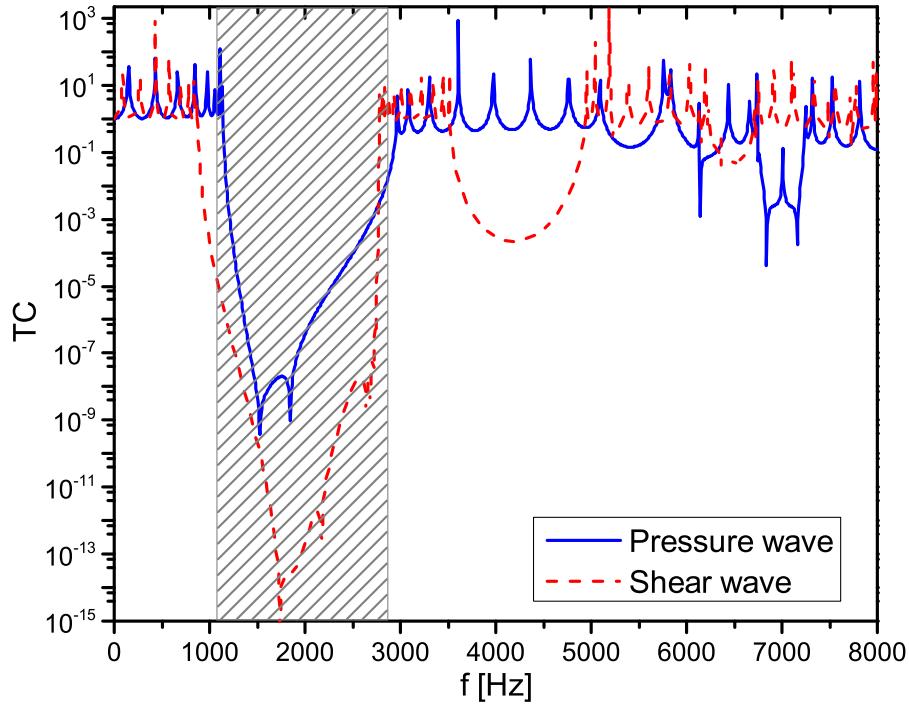
Acknowledgements

Figure 14: Transmission coefficient of the melamine-aluminum in the finite media. The shaded area corresponds to the band gap obtained from the dispersion analysis.

References

[1] Z. Yang, J. Mei, M. Yang, N.H. Chan, P. Sheng, Membrane-type acoustic metamaterial with negative dynamic mass, Phys. Rev. Lett., 101 (2008) 204301.

[2] G. Ma, P. Sheng, Acoustic metamaterials: From local resonances to broad horizons, Sci. Adv., 2:2 (2016) e1501595.

[3] D. Lee, D.M. Nguyen, J. Rho, Acoustic wave science realized by metamaterials, Nano Converg., 4:3 (2017). https://doi.org/10.1186/s40580-017-0097-y.

[4] X. Man, T. Liu, B. Xia, Z. Luo, L. Xie, J. Liu, Space-coiling fractal metamaterial with multi-bandgaps on subwavelength scale, J. Sound Vib., 423 (2018) 322–339.

[5] X. Man, B. Xia, Z. Luo, J. Liu, 3D Hilbert fractal acoustic metamaterials: low-frequency and multi-band sound insulation, J. Phys. D Appl. Phys., 52:19 (2019) 195302.

[6] D. Gao, X. Zeng, X. Liu, K. Han. Resonant modes of one-dimensional metamaterial containing helmholtz resonators with point defect, J. Mod. Phys., 8 (2017) 1737–1747.

[7] C. Elachi, Waves in active and passive periodic structures: A review, Proc. IEEE, 64:12 (1977) 1666–1698.

[8] A. Singh, D.J. Pines, A. Baz, Active/passive reduction of vibration of periodic one-dimensional structures using piezoelectric actuators, Smart Mater. Struct., 13:4 (2004) 698.

[9] L. Zheng, Y. Li, A. Baz, Attenuation of wave propagation in a novel periodic structure, J. Cent. South Univ. T., 18:2 (2011) 438–443.
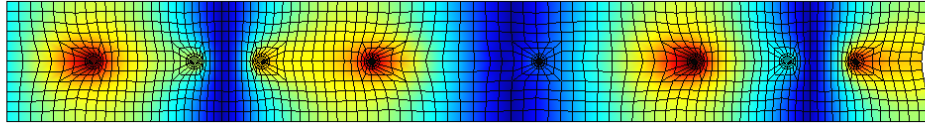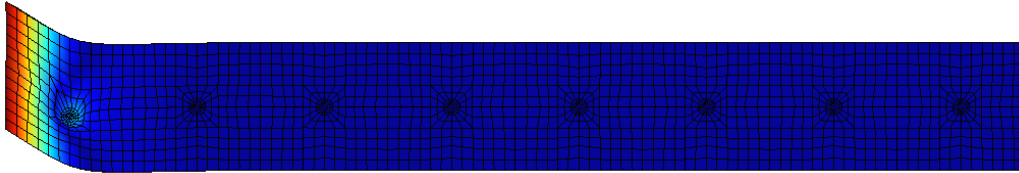
(a) Pressure wave - 792 Hz
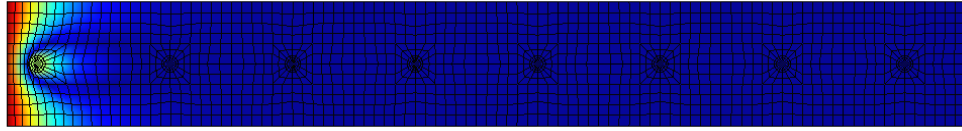
(b) Pressure wave - 1592 Hz
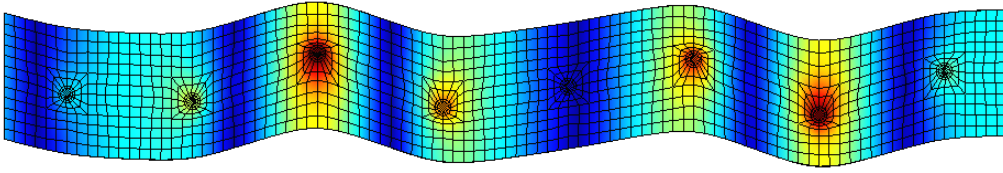
(c) Shear wave - 792 Hz

(d) Shear wave - 1592 Hz

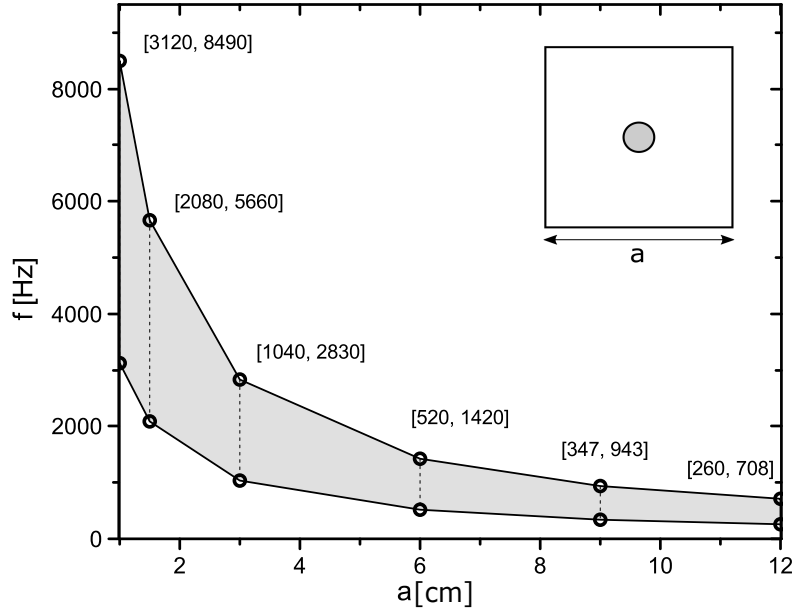Figure 15: Modes of the finite strip of cells at 792 Hz and 1592 Hz.

Figure 16: Evolution of the band gap size as function of the cell dimension. The numbers in brackets correspond to the lower and upper limits of the band gap for each dimension studied.

[10] A.C. Slagle, Low frequency noise reduction using poro-elastic acoustic metamaterials, in: PdD thesis, Virginia Polytechnic Institute and State University, 2014.

[11] A.C. Slagle, C.R. Fuller, Low frequency noise reduction using poro-elastic acoustic metamaterials, in: 21st AIAA/CEAS Aeroacoustics Conference, Dallas, TX, June 2015.

[12] M.S. Kushwaha, P. Halevi, G. Martinez, L. Dobrzynski, B. Djafari-Rouhani, Theory of acoustic band structure of periodic elastic composites, Phys. Rev. B, 49:4 (1994) 2313–2322.

[13] F. Kobayashi, S. Biwa, N. Ohno, Wave transmission characteristics in periodic media of finite length: multilayers and fiber arrays, Int. J. Solids Struct., 41 (2004) 7361–7375.

[14] S. Gonella, M. Ruzzene, Analysis of in-plane wave propagation in hexagonal and re-entrant lattices, J. Sound Vib., 312:1-2 (2008) 125—139.

[15] M.I. Hussein, M.J. Leamy, M. Ruzzene, Dynamics of phononic materials and structures: Historical origins, recent progress, and future outlook, Appl. Mech. Rev., 66 (2014) 040802.

[16] P. Langlet, A.-C. Hladky-Hennion, J.-N. Decarpigny, Analysis of the propagation of plane acoustic waves in passive periodic materials using the finite element method, J. Acoust. Soc. Am., 98:5 (1995) 2792—-2800.

[17] M. Cinefra, G. D'Amico, A.G. de Miguel, M. Filippi, A. Pagani, E. Carrera, Efficient numerical evaluation of transmission loss in homogenized acoustic metamaterials for aeronautical application, Appl. Acoust., 164 (2020) 107253.

[18] A. Garcia de Miguel, A. Pagani, W. Yu, E. Carrera, Micromechanics of periodically heterogeneous materials using higher-order beam theories and the mechanics of structure genome, Compos. Struct., 180 (2017) 484–496.

[19] M. Cinefra, A. Garcia de Miguel, M. Filippi, C. Houriet, A. Pagani, E. Carrera, Homogenization and free-vibration analysis of elastic metamaterial plates by CUF finite elements, Mech. Adv. Mater. Struct., (2019) 1–10. https://doi.org/10.1080/15376494.2019.1578005.

[20] M. Petrolo, E. Carrera, G. Giunta, Beam structures: classical and advanced theories, John Wiley and Sons, Chichester, UK, 2011.

[21] E. Carrera, M. Cinefra, M. Petrolo, E. Zappino. Finite Element Analysis of Structures through Unified Formulation, John Wiley & Sons, Chichester (UK), 2014.

[22] E. Carrera, M. Petrolo, Refined beam elements with only displacement variables and plate/shell capabilities, Meccanica (Mechanics), 47:3 (2012) 537–556.

[23] E. Carrera, A. Pagani, M. Petrolo, Component-wise method applied to vibration of wing structures, J. Appl. Mech., 80:4 (2013) art. no. 041012, 1–15.

[24] E. Carrera, A. Pagani. Free vibration analysis of civil engineering structures by component-wise models, J. Sound Vib., 333:19 (2014) 4597–4620.

[25] E. Carrera, A. Pagani, M. Petrolo, E. Zappino, Recent developments on refined theories for beams with applications, Mech. Eng. Rev., 2:2 (2015) 14–00298.

[26] E. Carrera, M. Petrolo, A. Varello, Advanced beam formulations for free vibration analysis of conventional and joined wings, J. Aerospace Eng., 25:2 (2012) 282–293.

[27] M. Cinefra, Free-vibration analysis of laminated shells via refined mitc9 elements, Mech. Adv. Mater. Struct., 23:9 (2016) 937–947.

[28] L. Brillouin, Wave propagation in periodic structures, second edition, Dover Publications, New York, 1953.

[29] Y.F. Wang, Y.S. Wang, L. Wang, Two-dimensional ternary locally resonant phononic crystals with a comblike coating, J. Phys. D: Appl. Phys., 47, December 2014.

[30] Y.F. Wang, Y.S. Wang, V. Laude, Wave propagation in two-dimensional viscoelastic metamaterials, Phys. Rev. B, 92 (2015) 104110.

[31] K.E. Heitman, J.S. Mixson. Laboratory study of cabin acoustic treatments installed in an aircraft fuselage, J. Aircr., 23:1 (1983) 32–38.

[32] J.S. Mixson, L.A. Roussos, C.K. Barton, R. Vaicaitis, M. Slazak, Laboratory study of add-on treatments for interior noise control in light aircraft, J. Aircr., 20:6 (1983) 516–522.

[33] L.D. Pope, E.G. Wilby, C.M. Willis, W.H. Mayes. Aircraft interior noise models: Sidewall trim, stiffened structures, and cabin acoustics with floor partition, J. Sound Vib., 89 (1983) 371–417.

[34] M.J. Crocker. Handbook of Noise and Vibration Control, John Wiley & Sons, Inc. Hoboken, 2007.

[35] M.C. Moruzzi, M. Cinefra, S. Bagassi, Vibroacoustic analysis of an innovative windowless cabin with metamaterial trim panels in regional turboprops, Mech. Adv. Mater. Struct., doi:10.1080/15376494.2019.1682729 (2019) 1–13.

[36] C.R. Fuller, M.R.F. Kidner, X. Li, C.H. Hansen, Active-passive heterogeneous blankets for control of vibration and sound radiation, in: Proceedings of ACTIVE 2004, pages 20–24, Williamsburg, Virginia, USA, September 2004.

[37] M.R.F. Kidner, B. Gardner, C.R. Fuller, Improvements in low frequency insertion loss blankets: experimental investigation, J. Sound Vib., 294:3 (2006) 466–472.

[38] J. Cuenca, C. Van der Kelen, P. Goransson, A general methodology for inverse estimation of the elastic and anelastic properties of anisotropic open-cell porous materials - with application to a melamine foam, J. Appl. Phys., 115:8 (2014) 084904.

[39] L. Jaouen, A. Renault, M. Deverge, Elastic and damping characterizations of acoustical porous materials: Available experimental methods and applications to a melamine foam, Appl. Acoust., 69:12 (2018) 1129–1140.

[40] E. Carrera, A. Pagani, Accurate response of wing structures to free-vibration, load factors, and nonstructural masses, AIAA J., 54 (2016) 227–241.

[41] A.G. de Miguel, I. Kaleel, M.H. Nagaraji, A. Pagani, M. Petrolo, E. Carrera, Accurate evaluation of failure indices of composite layered structures via various FE models, Compos. Sci. Technol., 167 (2018) 174–189.

[42] A.G. de Miguel, A. Pagani, E. Carrera, Higher-order structural theories for transient analysis of multi-mode Lamb waves with applications to damage detection, J. Sound Vib., 457 (2019) 139–155.

[43] G. Li, A.G. de Miguel, A. Pagani, E. Zappino, E. Carrera, Finite beam elements based on Legendre polynomial expansions and node-dependent kinematics for the global-local analysis of composite structures, Eur. J. Mech. A Solids, 74 (2019) 112–123.

[44] G. Li, E. Carrera, M. Cinefra, A.G. de Miguel, A. Pagani, E. Zappino, An Adaptable Refinement Approach for Shell Finite Element Models Based on Node-Dependent Kinematics, Compos. Struct., 210 (2019) 1–19.

[45] B. Assouar, M. Oudich, X. Zhou, Acoustic metamaterials for sound mitigation, CR Phys., 17:5 (2016) 524–532.

Table 3: First 30 natural frequencies of the metamaterial unit cell made of melamine and aluminium.

$Freq.[Hz]$	CUF	Ansys
$dofs$	2798	59160
1	0.5078E+3	0.5068E+3
2	0.7135E+3	0.7124E+3
3	0.9039E+3	0.9018E+3
4	0.9365E+3	0.9460E+3
5	0.1233E+4	0.1235E+4
6	0.1536E+4	0.1532E+4
7	0.1538E+4	0.1548E+4
8	0.1667E+4	0.1701E+4
9	0.1721E+4	0.1723E+4
10	0.1766E+4	0.1761E+4
11	0.1234E+4	0.1234E+4
12	0.1536E+4	0.1532E+4
13	0.1538E+4	0.1548E+4
14	0.1667E+4	0.1701E+4
15	0.1722E+4	0.1723E+4
16	0.1766E+4	0.1760E+4
17	0.1872E+4	0.1862E+4
18	0.2284E+4	0.2284E+4
19	0.2344E+4	0.2353E+4
20	0.2408E+4	0.2408E+4
21	0.2429E+4	0.2422E+4
22	0.2596E+4	0.2577E+4
23	0.2597E+4	0.2593E+4
24	0.2646E+4	0.2632E+4
25	0.2733E+4	0.2730E+4
26	0.3039E+4	0.3033E+4
27	0.3409E+4	0.3381E+4
28	0.3669E+4	0.3672E+4
29	0.3825E+4	0.3815E+4
30	0.3911E+4	0.3902E+4